A distinct circuit for biasing visual perceptual decisions and modulating superior colliculus activity through the mouse posterior striatum

Kara K. Cover, Kerry Elliott, Sarah M. Preuss & Richard J. Krauzlis*

Laboratory of Sensorimotor Research, National Eye Institute
Bethesda, Maryland 20892 USA

*Lead contact:
Richard J. Krauzlis: richard.krauzlis@nih.gov

Conflicts of interest: none.

Keywords: vision, rodent, mouse, tail of the striatum, visual attention, in vivo electrophysiology.

Abstract

The basal ganglia play a key role in visual perceptual decisions. Despite being the primary target in the basal ganglia for inputs from the visual cortex, the posterior striatum's (PS) involvement in visual perceptual behavior remains unknown in rodents. We reveal that the PS direct pathway is largely segregated from the dorsomedial striatum (DMS) direct pathway, the other major striatal target for visual cortex. We investigated the role of the PS in visual perceptual decisions by optogenetically stimulating striatal medium spiny neurons in the direct pathway (D1-MSNs) of mice performing a visual change-detection task. PS D1-MSN activation robustly biased visual decisions in a manner dependent on visual context, timing, and reward expectation. We examined the effects of PS and DMS direct pathway activation on neuronal activity in the superior colliculus (SC), a major output target of the basal ganglia. Activation of either direct pathway rapidly modulated SC neurons, but mostly targeted different SC neurons and had opposite effects. These results demonstrate that the PS in rodents provides an important route for controlling visual decisions, in parallel with the better known DMS, but with distinct anatomical and functional properties.

Introduction

The basal ganglia comprise a set of interconnected subcortical nuclei that govern a range of complex functions. The best-known functions are related to motor control. The striatum, the input nucleus of the basal ganglia, facilitates elements of action execution including movement[1], goal-directed action selection[2] and orienting to valued sensory stimuli[3]. However, deficits in sensory perception are noted in disorders of basal ganglia function, such as Parkinson's[4] and Huntington's[5] diseases. Moreover, a growing body of evidence implicates the basal ganglia in aspects of perceptual decision-making that are distinct from motor control[6].

Sensory information is routed to the striatum through cortical and thalamic nuclei associated with somatosensory, visual, and auditory modalities[7,8]. The majority of studies on striatal involvement in visual perceptual behavior have focused on the dorsomedial striatum (DMS) in rodents and the head of the caudate nucleus in primates which receive input from visual cortex[9,10] as well as visual thalamus[11,12]. Dopamine D1-receptor expressing medium spiny neurons (D1-MSNs) in the striatum initiate the direct pathway, a disynaptic circuit that is believed to gate behaviors by disinhibiting basal ganglia targets in the thalamus and midbrain. Activating DMS D1-MSNs in mice biases visual decisions in a manner linked to the allocation of spatial attention[13,14]. Thus, several lines of evidence have established the direct pathway arising from the dorsal striatum as an important circuit for visual perceptual decisions.

The posterior striatum (PS) is also innervated by visual cortex and thalamus[8,9,15,16]. In the primate homologue, the tail of the caudate nucleus, neurons in the direct pathway encode visual cue value and bias the generation of saccades[17–19]. In

the rodent, a role for PS in visually guided behavior remains untested. PS D1-MSN signaling is causally involved in auditory decisions in mice[20,21]. Also, dopamine axons in the PS respond to light[22]. It thus seems plausible that visual circuits through the PS could be a major contributor to visual perceptual function, but this has yet to be explored in rodents.

Here, we investigated a functional role for the PS direct pathway in visual perceptual decisions. We first characterized this circuit using anatomical methods, and then tested its functional role by combining optogenetic PS or DMS D1-MSN manipulations with SC neuronal recordings in mice making visual decisions. We found that the direct pathway from the PS is largely segregated from that of the DMS and is more broadly and inclusively innervated by visual cortex. Activation of this PS direct pathway circuit biased performance in the visual change-detection task and modulated the activity of SC neurons. Whereas the predominate neuronal effect of PS or DMS D1-MSN activation was excitatory modulation of SC units, PS D1-MSN stimulation induced inhibitory effects more frequently than that of DMS. Together, these findings demonstrate that the PS provides a functionally significant and distinct route through the basal ganglia for visual perceptual decisions.

Results

The posterior striatum provides a unique basal ganglia direct pathway for visual signals

The rodent striatum is canonically divided into dorsomedial, dorsolateral, ventral, and posterior (or tail) subregions. D1-MSNs populate all regions of the striatum and provide the origin of the direct pathway of the basal ganglia. We sought to examine

whether the direct pathway originating from the PS is anatomically distinct or shared with that of the DMS. To do this, we expressed cre-dependent anterograde fluorophore -expressing viruses in the PS and DMS of Drd1a-cre heterozygous mice (Figure 1A-D). We found that DMS labeled D1-MSNs terminated in the ventral medial segment of the substantia nigra (SN) and in the entopeduncular nucleus (EP; homolog to the primate internal segment of the globus pallidus). In contrast, PS labeled D1-MSNs innervated the dorsal lateral region of the SN, with no labeling in the EP.

We then used a viral strategy to selectively label the neurons in the SN that are postsynaptic to PS and DMS D1-MSNs. We injected anterograde trans-synaptic AAV1 viruses in the PS and DMS of wild-type mice that delivered cre or flp recombinases to all efferent cells. We then co-injected cre- and flp-dependent fluorophore-expressing viruses in the SN to locally label all recombinase-expressing cells (Figure 1E-L). We found that neurons targeted by DMS D1-MSNs resided nearly exclusively in the substantia nigra pars reticulata (SNr) and in the overlying substantia nigra pars compacta (SNc). In contrast, neurons targeted by PS D1-MSNs were largely confined to the substantia nigra pars lateralis (SNl) and adjacent peripeduncular nucleus (PP). Only a couple of cells showed dual-fluorophore labeling, indicating that the direct pathways originating from the PS and DMS are largely segregated. By following the axonal expression of the neurons targeted by the PS and DMS D1-MSNs, we found a mixture of both exclusive and shared output targets in the thalamus, midbrain, and striatum. In a separate set of cases, we applied this di-synaptic labeling approach to confirm the projection from DMS D1-MSNs to neurons in the EP, with axons that innervate several midbrain nuclei and the habenula (Figure 1M-P).

Although pathways originating in both DMS and PS innervate the SC, we observed striking differences. DMS-originating terminals showed concentrated innervation of SC intermediate layers and stronger innervation in more rostral sections of the SC, whereas PS-originating terminals exhibited a more diffuse innervation across intermediate and deeper layers and relatively stronger expression in more caudal sections of the SC.

Having established that D1-MSNs in the PS and DMS give rise to anatomically distinct pathways through the basal ganglia, we next compared the extent of visual cortical innervation to these two striatal subregions. Prior work indicates that the PS and DMS are the exclusive striatal targets of visual cortex[8]. To identify the regions of visual cortex that project to these striatal regions, we injected the retrograde tracer Fluorogold unilaterally in either the PS or DMS of wild-type mice. We observed strong labeling of PS-projecting cells in what we identified as layers 5 and 6 across the entire rostral-caudal axis of the visual cortex, both in primary and secondary visual areas (Figure 2A-D). In contrast, we found strong labeling of DMS-projecting cells in layer 5 in rostral visual cortex but the labeling was weaker in more caudal sections, especially for primary visual cortex (Figure 2E-H). We also observed weak labeling of putative layer 3 cells for both striatal regions (PS, Figure 2B; DMS, Figure 2F). These findings agree with similar findings in rats demonstrating stronger innervation from the visual cortex and thalamus to the PS than to the DMS[23].

Stimulation of the posterior striatum biases visual decisions

Our neuroanatomical results establish that the PS direct pathway is a major route for visual signals through the basal ganglia and that this route is distinct from that provided by the DMS. We next probed for functional roles of this striatal region by optogenetically activating PS D1-MSNs in mice performing a spatially cued orientation change-detection task[14,24]. Briefly, head-fixed mice were presented a vertical Gabor patch cue in one visual field that drifted at a rate coupled to running speed (Figure 3A). As the trial proceeded, a second Gabor patch appeared in the opposite visual field. After a variable distance, the patch that had appeared first either changed orientation or remained vertical ('catch'; 50% occurrence for each). Mice were trained to report their detection of the orientation change by licking a centrally placed spout to receive a soymilk reward. Sessions were run in 40-trial blocks in which the orientation changed occurred exclusively in one visual field (left or right) before switching to the other location.

We unilaterally stimulated channelrhodopsin (ChR2)-mCherry -expressing PS or DMS D1-MSNs in Drd1a-cre mice during one of three epochs of the task (Figure 3B-C). On 50% of the trials, 150 ms blue light was delivered either shortly after the appearance of the second Gabor patch ('early delay'), during the change event ('change'), or at a time-matched period on catch trials ('late delay'). The visual conditions were identical between the early delay and late delay conditions (the presence of two vertical Gabor patches). We assessed lick responses within 750 ms of light delivery onset (or an equivalent time window on no-stimulation trials).

Light delivery to the PS during the early delay produced a small but significant increase in lick probability ('yes' response) in ChR2-mCherry-expressing mice (N = 6)

compared to non-stimulation trials (Figure 3D-E; Table 1). Delivering light to the PS of mice expressing a control mCherry fluorophore (mCherry; N = 4) did not result in significant changes in lick probability (Figure 3E; Table 1). Delivering light during the late delay induced a larger significant increase in lick probability for ChR2-mCherry mice (Figure 3D,F, Table 1). Again, the control mCherry mice showed no effect (Figure 3F; Table 1). Comparing the effects across the factors, repeated measures 4-way ANOVA revealed significant main effects for epoch, light delivery, and group, but not cued side, and included several significant interactions across factors (Table 1). Thus, our main finding with optogenetic stimulation during the delay period of the task was that light-evoked increases in lick probability were significantly greater during the late delay than the early delay.

For light delivered to the PS during the change event, because performance was already at ceiling, it was not possible to observer increases in lick rate. However, we did find effects on lick reaction time. Delivering light to the PS during the change event significantly reduced the median response latency in ChR2-mCherry mice but not in mCherry control mice (Figure 3G; Table 2). A repeated measures 3-way ANOVA showed a significant main effect of light delivery, but not of group nor cued side (Table 2).

Comparison with stimulation of the dorsomedial striatum

In the same mice, we also tested the effects of DMS direct pathway stimulation during the task. Our group previously demonstrated that DMS D1-MSN activation biases lick responses in a manner dependent on spatial cues and reward conditions[13,14]. Here, to compare with our PS activation, we tested whether temporal

expectation also influenced the behavioral effects of DMS direct pathway activation. We found that light delivery to the DMS during the early delay did not significantly change lick probability for either ChR2-mCherry mice or mCherry control mice (Table 1). Light delivery to the DMS during the late delay did significantly increase lick probability in ChR2-mCherry mice but not mCherry control mice (Table 1). As with PS, a repeated measures 4-way ANOVA revealed significant main effects for epoch, light delivery, and group, but not cued side, and included several significant interactions (Table 1).

We also examined the effects of DMS direct pathway stimulation on the response to the change event. Unlike our results with PS stimulation, we did not find a significant effect of light delivery on median response latency for ChR2-mCherry mice or mCherry mice (Table 2). A repeated measures 3-way ANOVA revealed a trending but insignificant main effect of light delivery (Table 2).

Thus, stimulation of either the PS or DMS biased decisions in our visual change-detection task, and both showed larger effects when the stimulation was applied late in the delay period, when the change event was expected to occur. These results show that stimulation of either PS or DMS does not automatically evoke a lick response, but instead depends on the context and temporal structure that the mice have learned to associate with rewards in our visual task.

Effects of stimulating PS and DMS depend on the visual context and reward reinforcement

To further elucidate the conditions in which PS direct pathway activation biases visual decisions we performed two additional behavioral experiments in the same

cohort. First, we tested whether the induced lick response depended on the presence of choice-relevant visual stimuli. Using our standard visual change-detection task, we introduced a minority of trials in which the stimulation was paired with either the one-patch or pink noise stimuli, but at a time temporally matched to stimulation during the late delay or change epoch (Figure 4A *left*). This experiment replicated our earlier finding that stimulation during contralaterally cued two-patch visual presentation increased the mean lick probability (no light: 0.067 ± 0.034 s.e.m. vs. light: 0.491 ± 0.044). In contrast, pairing PS D1-MSN activation with the contralateral one-patch stimulus resulted in a lick probability of 0.249 ± 0.054, approximately half as much as the two-patch, and light delivery paired with pink noise produced a lick probability of 0.018 ± 0.012, essentially zero (Figure 4A *right*). A repeated measures 1-way ANOVA showed a significant main effect of visual stimulus ($F(3,15) = 40.17$, $P < 0.0001$) on lick probability. Thus, the effects of PS stimulation were not simply due to timing in the task but depended on the presence of the combination of visual stimuli signaling the possibility of a reward-related event.

We next asked whether the decision bias mediated by PS stimulation also depended on reward reinforcement. Specifically, if rewards were withheld for correct responses in our visual task, would PS D1-MSN activation still evoke licks, or otherwise delay the emergence of operant extinction? To test this, we ran mice on a modified version of the task in which only contralaterally cued trials were presented (50% resulted in the change event; 50% of both trial types were paired with PS D1-MSN stimulation). After 60 trials in which correct detection responses were rewarded, trials continued as before but with no rewards administered for the remainder of the session

(Figure 4B *left*). Pooling across 10 sessions from 4 mice, we quantified the extinction rates separately for non-stimulation and PS D1-MSN stimulation trials by fitting the hits and misses relative to the first non-rewarded trial in a four-parameter logistic regression model with bootstrapped computed 95% confidence intervals (CIs) (Figure 4B *right*). We found that the fitted model curve for stimulation trials did not significantly differ from that of non-stimulation trials. A predicted hit rate of 0.5 occurred at 8.9 trials (95% CIs: 5, 11.8) post- reward non-reinforced on the curve fitted to the non-stimulation trials and 5.8 trials (CIs: 1.4, 9.1) on the curve fitted to stimulation trials (z-test z = -1.673, P = 0.094). Thus, PS stimulation did not change the time course of operant extinction, and the effects of PS stimulation disappeared as extinction took hold.

The basal ganglia direct pathway modulates superior colliculus neuronal activity during visual decision-making

Having demonstrated that both PS and DMS D1-MSN activation robustly affects visual decisions in our task, we next investigated one of the major output targets of these basal ganglia circuits and how neuronal activity was modulated during the visual detection task. The SC is a shared target of both PS- and DMS-originating direct pathways (Figure 1 K,L,O,P) and plays a crucial role in visual processing and visually guided decisions in rodents[25,26]. We collected extracellular electrophysiological recordings in the SC of our cohort of PS and DMS D1-MSN ChR2-mCherry expressing mice (N = 6) performing the orientation change-detection task with and without optogenetic stimulation. PS or DMS D1-MSN activation was tested in separate recording sessions.

We recorded a total of 530 single units across the layers of the SC (Figure 5A). Grouping these units by their estimated location in either superficial (sSC) or deeper (dSC) layers, we observed neuronal responses to key features of the spatially cued change-detection task (Figure 5B-C; Table 3). Phasic responses to the onset of the cue patch, when presented in the contralateral visual field, were present in the majority of SC neurons: 78.4% of sSC units and 55.7% of dSC units. Delay activity (defined as a significant difference in firing rates in the late vs early delay epochs) was also observed in many neurons: 46.6% of sSC units and 37.3% of dSC units. We observed spatial cue-related modulation (defined as the difference in firing rate between contra- and ipsi-laterally cued trials late in the delay epoch) but this was present in a minority of neurons: 18.2% of sSC units and 20.6% of dSC units. Similarly, phasic responses to the orientation change were observed in 18.2% of sSC units and 22.4% of dSC units. Lastly, we found lick-related activity (defined as the difference in firing rate in a 100 ms window centered on the first detection lick compared to pre-change event firing activity) in a small minority of SC neurons: 1.1% of sSC units and 6.6% of dSC units. Comparing the modulation between the superficial and deep layers, we found that sSC units were significantly more likely to have a cue response than dSC units ($\chi^2 = 15.76$, $P < 0.0001$) whereas dSC units were significantly more likely to have lick-related activity ($\chi^2 = 4.04$, $P = 0.044$).

We next identified how SC units that exhibited these different task-related properties were modulated by stimulation of the direct pathways originating in PS and DMS. We classified units as being modulated by D1-MSN activation if there was a significant difference in firing during the 150 ms light-delivery period compared to an

equivalent window during non-stimulation trials, for the early and late delay epochs. For the sSC, we found very few units to be modulated by either PS (4 out of 35 units) or DMS (3 out of 45 units) D1-MSN activation. Therefore, we restricted our analyses to dSC units, among which 51 out of 186 units were modulated by PS direct pathway activation and 83 out of 228 units were modulated by DMS direct pathway activation.

We observed that activation of the striatal direct pathways did not affect all dSC units equally. For the PS, we found that D1-MSN activation was more likely to modulate units that exhibited delay activity ($\chi^2 = 4.46$, $P = 0.035$), showed spatial cue-related modulation ($\chi^2 = 5.92$, $P = 0.015$), or responded to the orientation change ($\chi^2 = 16.74$, $P < 0.0001$) (Figure 5D *left*; Table 3). Similarly, for the DMS, D1-MSN activation preferentially modulated units with delay activity ($\chi^2 = 9.52$, $P = 0.002$), spatial cue-related modulation ($\chi^2 = 12.66$, $P = 0.0004$), or that responded to the orientation change ($\chi^2 = 17.89$, $P < 0.0001$). DMS D1-MSN activation was also more likely to modulate units that did not show lick related activity ($\chi^2 = 6.60$, $P = 0.0102$) (Figure 5D *right*; Table 3).

Because the basal ganglia direct pathway reaches the SC by a series of two inhibitory projections, we expected activation of D1-MSNs to have a predominately excitatory effect on SC neuronal activity[1,27–29]. Indeed, the majority of units modulated by PS or DMS direct pathway activation showed excitatory changes in firing rate (Figure 5D *dark bars*; Figure 6A *left*; Figure 6B *left*). However, we also observed populations of units that were exclusively inhibited by direct pathway activation (Figure 5D *light bars*; Figure 6A *middle*; Figure 6B *middle*). This effect was more prevalent for PS: stimulation induced an inhibitory effect in a larger percentage of dSC units modulated by PS

(27.5%; 15.9, 41.7 95% CI) than modulated by DMS (13.3%; 6.8, 22.5; $\chi^2 = 4.20$, P = 0.04). Finally, we observed a small number of units that demonstrated both excitation and inhibition, either in different test epochs or within the same epoch (Figure 5D *mid-tone bars*; Figure 6A *right*; Figure 6B *right*).

We also examined whether dSC modulation by direct pathway activation depended on the stimulated epoch. For PS stimulation, we found that approximately half of D1-MSN modulated dSC units were modulated during both the early and late delay epochs (54.9%), whereas 39.2% were exclusively modulated during the early delay and only a small percentage were modulated exclusively during the late delay (5.9%) (Figure 6C). dSC units modulated by DMS D1-MSN stimulation showed similar distributions: 48.2% for both epochs, 45.8% exclusively during the early delay, and 6.0% exclusively during the late delay (Figure 6C).

Direct comparison of PS and DMS activation on SC unit activity

We also were able to directly compare the effects of PS and DMS direct pathway activation on SC units. This comparison at the neuronal level is of particular interest because our histological tracing of PS and DMS direct pathways targeting the SC showed distinct but overlapping patterns of axonal innervation in the SC. We investigated whether these pathways target the same neuronal populations within the SC. In two mice, we recorded from SC units while stimulating PS or DMS D1-MSNs during the early delay in the same session. We recorded a total of 30 optogenetically modulated single units: 40% were exclusively modulated by DMS direct pathway activation, 20% were exclusively modulated by PS direct pathway activation, and 40%

were modulated by both pathways (Figure 6D). Of the units that were modulated by both direct pathways, 58.3% exhibited different modulatory effects, that is, these units were excited by one pathway and inhibited by the other. Together, these findings indicate that although some SC units are targeted by both PS and DMS direct pathways and exhibit similar modulatory effects, the majority of SC units we recorded (83.3%) showed differential effects – they were either modulated by only the DMS or PS, or if they were modulated by both, they exhibited opposing modulatory effects.

Discussion

The present study investigated the contributions of the mouse PS to visual behavior. Our results demonstrate that the PS is uniquely anatomically positioned to relay visual signals through the basal ganglia. Compared to the DMS, which has been studied more frequently in visual tasks, the PS is more strongly innervated by visual cortex and gives rise to an alternative set of direct pathways for visual processing. Our results show that activating these direct pathways robustly and selectively modulates visual decisions. We also identified that both PS and DMS direct pathway activation targeted neurons in the SC that were sensitive to context and reward-associated stimuli. Together, these findings further demonstrate distinct circuits through the basal ganglia for visual perceptual decision-making.

Our findings join several lines of research implicating the basal ganglia in perceptual decision-making. In the primate homologue of the dorsal striatum, caudate neurons exhibit spatially selective modulation in the absence of goal-directed actions[30]. Neurons in the caudate of primates[31] and dorsal striatum of rats[32] show activity

consistent with sensory evidence accumulation. Our group has previously shown that activating the DMS direct pathway selectively biases responses for expected contralateral visual events[13,14]. These findings collectively suggest that the basal ganglia have a distinct role in promoting perceptual decisions separable from the decision motor output.

Our results here illustrate that stimulating the PS direct pathway does not drive an obligatory and fixed motor response. Optogenetic activation induced ‘yes’ perceptual responses that depended on visual and temporal context. Moreover, PS D1-MSN stimulation did not delay extinction of the response to the devalued change event when rewards were withheld. Our observation that activation of PS and DMS direct pathways failed to modulate the vast majority of SC units that exhibited lick-related activity further supports the absence of effects directly on motor circuits. Instead, our findings support a conceptual understanding of the striatum in providing a permissive gating function for pre-selected actions[33]. In the context of perceptual decision-making, the convergence of cortical and subcortical inputs to the striatum is proposed to enable the selection and evaluation of sensory decision policies[6].

The effects of PS direct pathway manipulation on visual decisions were similar to that of the DMS[14], suggesting a comparable influence on perceptual behavior. However, anatomical differences hint at potential functional differences between these striatal subregions. The DMS was preferentially innervated by anterior primary and secondary visual areas. Neurons in mouse anterior secondary areas are noted to preferentially respond to stimuli of lower spatial and higher temporal frequencies, exhibit stronger orientation selectivity, and prefer fast-moving stimuli[34]. In contrast, we found that the PS

was innervated by all of secondary visual cortex, including posterior areas that are characterized by a preference for lower spatial, higher temporal, and slow-moving stimuli[34]. Whether this broader anatomical connection confers the PS a relative sensitivity or contextual selectively for visual input remains to be determined.

Differences in striatal afferents extend beyond the visual cortex. Whereas the DMS is preferentially innervated by frontal cortices including anterior cingulate, prelimbic and orbital cortices, the PS notably receives input from all sensory cortical areas[8,16]. Accordingly, the PS direct pathway biases auditory decisions[20,21]. Dopaminergic signaling in this region reinforces the avoidance of novel or threatening stimuli of multiple sensory modalities[22] and is also shown to scale with auditory uncertainty[21]. Moreover, activating PS D1-MSNs in freely moving mice failed to induce orienting responses which are reliably observed with dorsal striatal direct pathway activation[20]. The combination of sensitivity to multimodal stimuli and distinct dopaminergic activity positions the PS to uniquely contribute to decision-making and behavior. Further characterization of striatal subregion involvement in more naturalistic paradigms may reveal distinct contributions of the PS and DMS to complex functions including visual perception.

Our tracing of PS and DMS direct pathways revealed a striking anatomical segregation through the basal ganglia output nuclei. The DMS direct pathway routed through the SNr and EP, whereas the PS direct pathway innervated the SNl and PP. Whereas characterization of the basal ganglia direct pathway has largely centered on the circuits through the SNr[35], the lesser studied output nuclei facilitate basal ganglia driven behavior as well. The EP consists of heterogeneous neuronal populations that

target different thalamic, habenular, and midbrain structures[36–38]. Activity in the primate homologue of the EP is modulated by reward-associated visual stimuli[39] and reflects rewarded voluntary movements[40]. In rodents, the EP's projection to the habenula contributes to valence-encoding[41] and the learned aversive response to cocaine[42]. Whether the DMS direct pathways through the EP and SNr provide distinct contributions to visual decisions is unknown.

Our findings of robust behavioral effects induced by PS D1-MSN activation suggest that the SNl and/or PP also play a role in perceptual decision-making. The few published studies of these nuclei primarily examined anatomical properties. The SNl consists of dopaminergic and GABAergic neurons that differentially project to sensory nuclei (i.e., SC, lateral posterior thalamus, inferior colliculus), motor-related regions (i.e., ventral anterior thalamus, reticular formation), the amygdala, as well as forming loops back to the basal ganglia[43–46]. The adjacent PP innervates the SC, inferior colliculus, pons, amygdala, basal ganglia nuclei, zona incerta, hypothalamus, and ectorhinal cortex[47,48]. The PP is associated with sexual and maternal behaviors[49,50], and the SNl and PP have been collectively proposed to mediate an anti-convulsant function[51]. Deep brain stimulation of the PP is also shown to improve motor deficits in severe Parkinson's disease[52,53]. How these output nuclei specifically facilitate perceptual decision-making functions remains to be determined.

Our SC recordings point to differences in the neuronal populations targeted by the DMS and PS basal ganglia pathways. We observed that PS direct pathway activation induced inhibition in a relatively larger population of dSC units. Given the established disinhibitory effect of the direct pathway, excitation was the expected, and

indeed, predominate modulatory effect on SC unit firing. However, suppression may occur if the recorded SC unit is efferent to a local interneuron that is itself disinhibited by the direct pathway resulting in a tri-synaptic inhibitory configuration (e.g., D1-MSN→SN/EP→SC interneuron→recorded SC unit). A larger proportion of SC units inhibited by PS D1-MSN activation may suggest that this direct pathway innervates SC interneurons more than that by the DMS. Our direct comparisons of SC neuronal modulation to both PS and DMS D1-MSN activation further supports the interpretation that these direct pathways target different neuronal populations. Of the dSC units that were modulated by both pathways, more than half of the units were differently modulated by optogenetic activation.

Despite these differences, we found that both PS and DMS direct pathways preferentially modulated dSC units with specific types of task-related activity. Units that exhibited delay-related activity, spatial cue-related modulation, or phasically responded to the reward-associated orientation change were more likely to be modulated by PS and DMS direct pathway activation. Interestingly, we did not find a similar preference for units that responded to the appearance of the Gabor patch cue. This suggests that the direct pathway bias is not merely for visually responsive SC units, but for those processing aspects of visual signals related to a goal or outcome. Our group has previously shown that dSC cue-related modulation contributes to spatial attention by biasing signal processing for reward-associated event locations[54]. Preferential innervation of neurons showing attention-like activity may be one mechanism by which the direct pathway biases decisions in manner linked to the allocation of spatial attention[13].

The results of the present study provide the first evidence for involvement of the mouse PS in visual behavior. Here, we monitored the neuronal modulation of one target of the basal ganglia direct pathway, the SC, during a visual decision-making task. In addition to the several circuit routes comprising the direct pathway that we have already noted, there are also many output targets that may contribute to perceptual decisions, in addition to the superior colliculus. The basal ganglia direct pathway also targets the motor thalamus, reticular formation, and pedunculopontine nucleus, which may each also contribute to the behavioral response[55,56]. The specific combination of basal ganglia targets that get recruited likely depends on the types of sensory information involved and the motor response required[57]. In addition to the direct pathways, there are also indirect pathways arising from striatal D2-MSNs that contribute to the regulation of visual behaviors through circuit interactions that are still being uncovered. Indeed, an indirect pathway arising from the PS is implicated in multi-sensory attentional filtering[58]. Although it remains an open challenge to understand how these complex circuits operate together for visual perception, our results show that any description should include circuits that originate in the posterior striatum.

Methods

Subjects

Male and female C57BL/6J (wild-type; Jackson Laboratory, #000664) or Drd1a-Cre heterozygous (B6.FVB(Cg)-Tg(Drd1a-cre)EY217Gsat/Mmucd; MMRRC #034258-UCD) mice were housed a in temperature and humidity-controlled vivarium under a 12-hour reversed light/dark cycle (lights off at 0800 hours). All experimental procedures

occurred during the dark cycle. Mice were housed with littermates (two to five per cage), except for those singly housed following head post and optic fiber implantation. Mice performing behavioral tasks were weighed and fed daily to maintain (at least) 85% *ad libitum* weight and the health status of each mouse was monitored daily throughout the study. These mice had free access to water, but their intake of dry food was controlled and were additionally given access to a nutritionally complete 8% soy-based infant formula (Similac, Abbott, IL). For behavioral experiments, animals were randomly assigned to control and experimental groups. Group assignment was also balanced to ensure equal numbers of males and females. All experimental and animal husbandry procedures were approved by the NIH Institutional Animal Care and Use Committee (IACUC) and complied with the Public Health Service policy on the humane care and use of laboratory animals.

Surgical procedures

Mice of at least 6 weeks of age were anesthetized with isoflurane (4% induction, 0.8-1.5% maintenance) and secured by a stereotaxic frame with ear bars. A feedback-controlled heating pad was used to maintain the body temperature at 37°C and ophthalmic ointment was applied to the eyes. Dexamethasone (1.6 mg/kg, s.c.) and meloxicam (2.0 mg/kg, s.c.) were administered to reduce inflammation and discomfort, respectively. Viruses were infused at a rate of 2 nl/s (50 nl/min maximum) using a microinjector (Nanoject III, Drummond Scientific, Broomall, PA).

For basal ganglia direct pathway tracing in Drd1-cre heterozygous mice, either AAV1-Ef1A-DIO-iChloc-2a-dsRed (NIDA Genetic Engineering and Viral Vector Core) or AAV1-Ef1A-DIO-eYFP (Addgene #27056-AAV1) was unilaterally injected in the DMS

(200 nl; distance from bregma in mm, [anterior-posterior, AP] 0.0, [medial-lateral, ML] 2.0, [dorsal-ventral, DV] -2.1) and the other virus injected in the PS (100 nl at each depth; [AP] -1.5, [ML] 3.5, [DV] -2.5 and -3.1). The viruses injected in DMS and PS were counter-balanced across 3 mice.

For di-synaptic tracing of DMS and PS direct pathways through the SN in wild-type mice, either AAV1-hSyn-cre-WPRE-hGHpA (Addgene #105553-AAV1) or AAV1-Ef1a-flp (Addgene #55637-AAV1) was unilaterally injected in the DMS and the other virus in the PS (same volumes and coordinates as listed above), as well as Fluorogold (30 nl, 1.5%, Fluorochrome LLC, Denver, CO) to label the injection site. In the same mice, both AAV1-Ef1a-fDIO-mCherry (Addgene #114471-AAV1) and AAV1-Ef1a-DIO-eYFP (Addgene #27056-AAV1) were injected in the SNR (150nl each; [AP] -3.2, [ML] 1.6, [DV] -4.4). The viruses injected in DMS and PS were counter-balanced across 4 mice. For di-synaptic tracing of the DMS direct pathway through the EP (200 nl; [AP] -1.25, [ML] 1.9, [DV] -4.3), a single set of viruses were used (either AAV1-cre and AAV1-DIO-eYFP, or AAV1-flp and AAV1-fDIO-mCherry), counter-balanced across 4 mice.

For retrograde tracing of projections to the striatum, Fluorogold (3%) was unilaterally injected in the DMS (80 nl; [AP] 0.0, [ML] 2.15, [DV] -2.1) of 2 mice or in the PS (40 nl at each depth; [AP] -1.5, [ML] 3.5, [DV] -2.5 and -2.95) of 2 mice.

For optogenetic manipulation of the direct pathway in mice performing behavioral tasks, AAV2-Ef1a-DIO-hChR2(H134R)-mCherry (University of North Carolina viral core) or a control virus AAV1-hSyn-DIO-mCherry (Addgene #50459-AAV1) was injected unilaterally in the DMS (250 nl; [AP] 0.0, [ML] 1.7, [DV] -2.1) and the PS (80 nl at each depth; [AP] -1.5, [ML] 3.25, [DV] -2.25 and -2.75). Additionally, optic fibers (200 µm core;

Plexon, Dallas, TX) were inserted in the DMS ([AP] 0.0, [ML] 1.7, [DV] -1.7) and PS ([AP] -1.5, [ML] 3.25, [DV] -2.15) and a custom-designed titanium head post was secured to the skull using Metabond (Parkell Inc., Edgewood, NY). The skin wound edge was then closed with surgical adhesive and treated with antibiotic ointment. Mice assigned to behavioral testing began food restriction 18-20 days following surgery.

After mice were trained and tested on the visual detection task with optogenetic manipulation, a second surgery was performed to implant electrophysiology microwire bundles. Following the same anesthetic and analgesic procedure as detailed above, a small craniotomy was made to implant a drivable 16-wire microwire bundle (Innovative Neurophysiology, Durham, NC). The tip of the stainless steel cannula of the bundle was implanted at [AP] -3.4 – -3.9, [ML] 0.8 – 1.2 and [DV] -0.2. The cranial opening was sealed with Vaseline petroleum jelly and the microwire bundle assembly was secured on the skull with Metabond.

Immunohistochemistry was performed to confirm virus expression and fiber placement. Animals were excluded from analysis for poor virus expression at target regions or viral expression in non-target regions (i.e. cortex).

Immunohistochemistry

Mice were deeply anesthetized with isoflurane prior to transcardial perfusion with 0.1 M PBS, pH 7.3, followed by ice cold 4% paraformaldehyde in PBS. Brains were extracted and stored in 4% paraformaldehyde at 4°C. 50 µm coronal sections were cut using either a Campden Instruments 7000smz-2 vibrating microtome (Lafayette, IN) at room temperature or, following transfer to 20% sucrose solution, a Leica SM2010 R freezing microtome (Deer Park, IL). Rabbit anti-GFP (1:1000; G10362, Invitrogen,

Carlsbad, CA) and donkey anti-rabbit conjugated to Alexa Fluor 488 (1:1000; A21206, Invitrogen) were used to amplify eYFP expression. Chicken anti-mCherry (1:2000; NBP2-25158, Novus Biologicals, Littleton, CO) and donkey anti-chicken conjugated to Alexa Fluor 594 (1:1000; 703-585-155, Jackson ImmunoResearch, West Grove, PA) were used to amplify dsRed and mCherry.

Behavioral testing

Behavioral apparatus

Behavioral testing was conducted in a custom-built booth that displayed visual stimuli on the left- and right-hand sides of the head-fixed mouse that was coupled to their locomotion on a custom-built Styrofoam linear wheel[59]. A pair of LCD displays (VS17287; ViewSonic, Brea, CA) were positioned at a 45° angle from the midline of the animal so that the displays were centered on the right or left eye and subtended by ~90° horizontal and ~55° vertical of the visual hemifield. The viewing distance from the mouse to the screen was ~27.5 cm. Sound-absorbent material lined the inside of the booth to reduce noise.

Experiments were controlled by a computer using a modified version the PLDAPS system[60], consisting of a Datapixx peripheral (Vpixx Technologies, Saint-Bruno, QC, Canada) and the Psychophysics Toolbox[61,62] for MATLAB (MathWorks, Natick, MA), controlled by MATLAB-based routines run on a PC running Ubuntu 18.04 or on a Mac Pro (Apple, Cupertino, CA). The Datapixx device provided autonomously timed control of analog and digital inputs and outputs synchronized to the visual display stimuli. A spout delivering liquid rewards was placed near the mouth of the mouse and lick contacts on the spout were detected by a piezo sensor using custom electronics. ~5

- 10 μL of 8% solution of infant formula were used as rewards for correct task performance and were delivered via a peristaltic pump.

Visual detection tasks

The detection task was modified from our previously published study[14]. Animals were run in daily sessions producing 153 to 421 trials, with data pooled across sessions. Experiments were organized in blocks of randomly shuffled trials. Each trial consisted of a sequence of epochs that were defined by the stimuli presented on the visual displays. Epoch durations were determined by either the randomized timing of the epoch or the time that it took for the mouse to travel a randomized distance on the wheel. Mice were trained to detect a change in the orientation of a Gabor patch visual stimulus, which the mouse reported by contacting the lick spout to receive a reward.

The trial sequence of the primary detection task consisted of four epochs (Figure 3A). The average luminance across each visual display in all epochs was 4 – 8 cd/m^2. In the first epoch ("Pink noise"), the uniform gray of the intertrial interval was changed to pink visual noise with a root mean square contrast of 3.3%. In the second epoch ("Gabor patch cue") a vertically oriented Gabor patch was added to the pink noise, centered on either the left or right visual display. The sinusoidal grating of the Gabor patch (93.7% Michelson contrast) had a spatial frequency of 0.1 cycles per degree and was modulated by a Gaussian envelope with a full width at half maximum of 18° (standard deviation = 7.5°). The phase of the grating was incremented in proportion to the wheel rotation and updated on every monitor refresh so that the sinusoidal pattern displaced on the screen matched the distance that the mouse traveled on the wheel. The Gabor patch on the left (right) drifted leftward (rightward), consistent with optic flow

during locomotion. The third epoch (“Delay epoch”) consisted of vertical Gabor patches appearing in both left and right visual displays. The stimuli in the fourth epoch depended on whether the trial was a “Change” or “Catch” condition; the two trial types were equally likely and randomly interleaved within a block. On Change trials, the Gabor patch on the same side as the patch present in second epoch changed its orientation (10-13°, depending on the mouse). The direction of the orientation change was clockwise for the left patch and counterclockwise for the right patch. On catch no-change trials, neither Gabor patch changed orientation, such that the epoch proceeded as a seamless extension of the previous delay epoch.

Mice were to lick the spout upon detection of a change in the orientation of the Gabor patch and otherwise withhold licking. Mice were required to lick within a 550 ms response window starting 220 ms after the onset of the orientation change to score a “hit” and receive a reward. If the mouse failed to lick within the window, the trial was scored as a “miss” and no reward was given. On catch trials, if the mouse licked with the same response window aligned on the no-change epoch onset, the trial was scored as a “false alarm” and was used to calculate lick probability rates across trial types. If the mouse correctly withheld licks during this window, the trial extended to include an additional “Safety” epoch in which the initially appearing Gabor underwent a 30° suprathreshold orientation change and the mouse could receive a reward by licking within a comparable response window. This safety epoch was intended to maintain motivation by rewarding mice for correct behavior without violating the task rule that they should lick only for orientation changes. False alarms or two or more premature

licks before the response window resulted in termination of the trial and a three second timeout.

In half of the trials, 465 nm blue light was delivered unilaterally to either the PS or DMS using an LED system (Plexon). For half of these trials, light was delivered during the delay epoch ("Early delay") for 150 ms, starting 200 ms after the onset of the epoch. For the remaining 50% of stimulation trials, light was delivered during the fourth epoch, either during catch ("Late delay") or change trials with equal frequency, for 150 ms, starting 50 ms after the onset of the epoch. Light power was set at a fixed intensity per striatal target per mouse to induce a non-saturating increase in lick probability (i.e., less that 100%) and ranged from 0.05 to 1.0 mW across the ChR2-expressing cohort. Similar light intensities were used for mice expressing the control mCherry fluorophore.

Trials were organized into alternating 40-trial blocks in which the orientation change occurred for either the left or right Gabor patch. Each block had an equal number of trials with and without orientation changes, and with and without optogenetic light delivery, all randomly shuffled. Each session started with a mini-block of 20 trials without light delivery trials which were excluded from behavioral analysis.

A "sequence arrested" control experiment consisted of blocks of 54 trials, 40 of which followed the standard four-epoch trial sequence: 20 with an orientation change (half of which were paired with optogenetic stimulation during the change) and 20 no-change catch trials (half of which were paired with optogenetic stimulation during the late delay catch epoch). Two additional trial types were introduced in which the visual sequence of epochs stopped once the trial reached a particular epoch: seven stopped at the single Gabor patch and seven stopped at the pink noise. These sequence-

arrested trials had the same durations and matched timing for optogenetic light delivery as the standard four-epoch trial sequence. We recorded 2-3 sessions per mouse with PS D1-MSN stimulation and pooled across sessions.

To test the interaction of PS D1-MSN stimulation on unreinforced change detection responses, we conducted a version of the detection task with four trial types: catch and change trials (50% of each), with stimulation during the change or late delay on half of each. Instead of blocks of trials switching between left- and right-side orientation changes, we only presented trials with the Gabor patch cue and orientation change occurring in the visual field contralateral to the hemisphere receiving optogenetic stimulation. After a 60-trial block in which correct change detection was rewarded with soymilk rewards, the remaining trials were unreinforced and the session was terminated after the mouse extinguished lick responses. We recorded 2-3 sessions per mouse and pooled across sessions and mice for subsequent analysis.

In vivo electrophysiology

In the cohort of Drd1a-cre mice expressing DIO-ChR2-mCherry and optic fibers in PS and DMS, we obtained electrophysiological recordings from isolated neurons in the SC while mice performed the orientation change detection task with optogenetic activation of PS and DMS D1-MSNs. The extracellular activity of SC neurons was recorded with microwire bundles. Electrophysiological signals were acquired through an RZ5D processor (Tucker-Davis Technologies, Alachua, FL) with spikes filtered between 0.3 and 5 kHz and sampled at 25 kHz. Single units were sorted offline using KiloSort[63]. The SC surface was determined based on the first visual responses detected while

advancing the microwire bundle. Sessions alternated between optogenetic stimulation of either PS or DMS D1-MSNs.

Visual receptive field maps were obtained at the end of every recording session, during which white circular disks (118.5 cd/m^2) of 10° in diameter were flashed against a gray background (7.2 cd/m^2) in the visual display contralateral to the recording side. We sampled visual locations pseudo-randomly drawn from a 3 x 7 isotropic grid that extended from -25° to 25° in elevation and 0° to 90° in azimuth of the contralateral visual field. An individual trial consisted of 8 consecutive 250 ms flashes, which flash followed by a 250 ms blank interval. At least 9 flash repetitions for each grid location were presented in each mapping session. Receptive fields of individual neurons were estimated from the mean spike counts 50 – 150 ms after the flash onset in each grid location, after subtracting baseline activity. The baseline in each trial was defined as the mean spike count within the 100 ms period before the presentation of the first flash. Baseline-subtracted mean spike counts were linearly interpolated between grid locations with 1° resolution using the *scatteredInterpolant* function in Matlab.

Following the last recording session, we performed electrolytic lesions to aid in histological reconstruction of bundle location within the SC. Under isoflurane anesthesia, 80 µA current was delivered for 7-10 s to two wires per bundle. Mice were administered meloxicam and perfused one week later.

Eye movement monitoring

To verify that changes in SC neuronal activity were not simply due to eye movements, a 120Hz video eye tracking system (ETL-200, ISCAN, Woburn, MA) was used to monitor eye position and pupil size of head-fixed mice during electrophysiology

experiments with optogenetic manipulation. The frequency of eye movements occurring in trials with and without optogenetic D1-MSN stimulation per stimulation site, per mouse, was statistically tested with chi-square tests.

Quantification and statistical analysis

Behavioral analyses

Lick probability was quantified separately for contralaterally and ipsilaterally cued trials and light delivery and no light delivery trials. Probability was calculated from the number of trials in which there were any licks within a 750 ms window starting at onset of light delivery for light delivery trials and a matched time window for non-light delivery trials (i.e. 200 ms to 950 ms from onset of the early delay epoch and 50 ms to 800 ms from the onset of the late delay catch epoch) divided by the total number of trials within the assessed trial condition, per mouse. Reaction time was calculated from the first lick following the orientation change per trial condition per mouse.

To compare behavioral extinction rates we separately fit binary responses (1 = hit, 0 = miss) to the orientation change for non-stimulation and PS D1-MSN stimulation trials using a four-parameter logistic regression model[64]:

$$y = \max + \frac{min - max}{1 + (\frac{x}{thresh})^{slope}}$$

In which *x* is the trial number relative to reward non-reinforcement (1 = the first unrewarded trial), *y* is the value of the function, *min* is the minimal value of the curve, *max* is the value of y at the lowest value of x, *thresh* is the inflection point, and *slope* is the slope of the function. The four parameter terms were fit to binary data by minimizing mean squared error. For each data set, 95% CIs for the four parameters were estimated using a standard bootstrap procedure with 1000 random draws. Significant differences

between the fitted curves for non-stimulation and PS stimulation trials were assessed with z-tests for specific values of y (probability of a hit).

Neuronal analyses

Firing rates for each neuron were summarized by counting spikes within 20 ms non-overlapping bins aligned to key task events and z-score normalized to the mean firing rate calculated from within-trial activity across the recorded session. Population peri-stimulus time histograms were generated from spike counts in 20 ms bins sliding in 1 ms intervals and normalized to z-scores, with error bars representing standard error.

Phasic responses to the Gabor patch cue were tested by either Wilcoxon signed rank test on spike counts in the interval 50 – 150 ms after Gabor patch cue epoch onset to spike counts -100 – 0 ms before Gabor patch cue epoch onset on contralaterally cued trials (relative to the recorded hemisphere) or Wilcoxon rank sum test on spike counts in the interval 50 – 150 ms after Gabor patch cue epoch onset on contralaterally cued trials and spike counts in the same interval for ipsilaterally cued trials. Delay-related activity was tested by Wilcoxon signed rank test on spike counts in the interval 200 – 300 ms after delay epoch onset to spike counts in the final 100 ms of the same epoch. Spatial cue -related modulation was tested by unpaired t-test of spike counts in the last 200 ms of the delay epoch on contralaterally cued trials to that of ipsilaterally cued trials. Phasic response to the orientation change was tested by Wilcoxon signed rank test of spike counts in the interval 50 – 150 ms after change epoch onset to -100 – 0 ms before change epoch onset on contralaterally cued trials. Lick related activity was tested by Wilcoxon signed rank test of spike counts in the interval -50 – 50 ms relative to first detection lick during the change epoch to spike counts in the interval -100 to 0

ms prior to change epoch onset. Significant differences in the proportions of units exhibiting task-related properties were assessed by chi-square tests.

SC neuronal responses to optogenetic direct pathway stimulation were tested by Wilcoxon signed rank test on spike counts in the interval 0 – 150 ms relative to light delivery to spike counts in a time-matched interval on non-stimulation trials and manually validated. Responses in each stimulation epoch (early and late delay, contralateral and ipsilaterally cued trials) were separately assessed for optogenetic modulation.

Statistical analyses

Statistical tests were performed with Matlab (R2022a and R2023a) or GraphPad Prism 10 (Boston, MA) software. Error bars in figures represent 95% CI or standard error of the mean as indicated in figure legends. 95% CIs in figure plots were generated with the *binofit* Matlab function. The value of N represents the number of animals and n represents the number of units. All statistical tests were conducted two-sided, when applicable. Significant post-hoc Holm-Ŝidàk tests for ANOVAs are indicated in the figures. All asterisks in figures indicate: * $p<0.05$, ** $p<0.01$, *** $p<0.001$, and **** $p<0.0001$.

References

1. Freeze, B. S., Kravitz, A. V., Hammack, N., Berke, J. D. & Kreitzer, A. C. Control of basal ganglia output by direct and indirect pathway projection neurons. *J. Neurosci. Off. J. Soc. Neurosci.* **33**, 18531–18539 (2013).
2. Tai, L.-H., Lee, A. M., Benavidez, N., Bonci, A. & Wilbrecht, L. Transient stimulation of distinct subpopulations of striatal neurons mimics changes in action value. *Nat. Neurosci.* **15**, 1281–1289 (2012).
3. Hikosaka, O. *et al.* Direct and indirect pathways for choosing objects and actions. *Eur. J. Neurosci.* **49**, 637–645 (2019).
4. Permezel, F., Alty, J., Harding, I. H. & Thyagarajan, D. Brain Networks Involved in Sensory Perception in Parkinson's Disease: A Scoping Review. *Brain Sci.* **13**, 1552 (2023).
5. Profant, O. *et al.* Auditory dysfunction in patients with Huntington's disease. *Clin. Neurophysiol. Off. J. Int. Fed. Clin. Neurophysiol.* **128**, 1946–1953 (2017).
6. Ding, L. Contributions of the Basal Ganglia to Visual Perceptual Decisions. *Annu. Rev. Vis. Sci.* **9**, 385–407 (2023).
7. Hintiryan, H. *et al.* The mouse cortico-striatal projectome. *Nat. Neurosci.* **19**, 1100–1114 (2016).
8. Hunnicutt, B. J. *et al.* A comprehensive excitatory input map of the striatum reveals novel functional organization. *eLife* **5**, e19103 (2016).
9. Khibnik, L. A., Tritsch, N. X. & Sabatini, B. L. A direct projection from mouse primary visual cortex to dorsomedial striatum. *PloS One* **9**, e104501 (2014).

10. Yeterian, E. H. & Pandya, D. N. Corticostriatal connections of extrastriate visual areas in rhesus monkeys. *J. Comp. Neurol.* **352**, 436–457 (1995).
11. Kamishina, H., Yurcisin, G. H., Corwin, J. V. & Reep, R. L. Striatal projections from the rat lateral posterior thalamic nucleus. *Brain Res.* **1204**, 24–39 (2008).
12. Smith, Y. & Parent, A. Differential connections of caudate nucleus and putamen in the squirrel monkey (Saimiri sciureus). *Neuroscience* **18**, 347–371 (1986).
13. Wang, L. & Krauzlis, R. J. Involvement of Striatal Direct Pathway in Visual Spatial Attention in Mice. *Curr. Biol.* **30**, 4739-4744.e5 (2020).
14. Wang, L., Rangarajan, K. V., Gerfen, C. R. & Krauzlis, R. J. Activation of Striatal Neurons Causes a Perceptual Decision Bias during Visual Change Detection in Mice. *Neuron* **97**, 1369-1381.e5 (2018).
15. Griggs, W. S. *et al.* Flexible and Stable Value Coding Areas in Caudate Head and Tail Receive Anatomically Distinct Cortical and Subcortical Inputs. *Front. Neuroanat.* **11**, 106 (2017).
16. Lee, K., An, S.-Y., Park, J., Lee, S. & Kim, H. F. Anatomical and Functional Comparison of the Caudate Tail in Primates and the Tail of the Striatum in Rodents: Implications for Sensory Information Processing and Habitual Behavior. *Mol. Cells* **46**, 461–469 (2023).
17. Kim, H. F., Amita, H. & Hikosaka, O. Indirect Pathway of Caudal Basal Ganglia for Rejection of Valueless Visual Objects. *Neuron* **94**, 920-930.e3 (2017).
18. Amita, H., Kim, H. F., Smith, M. K., Gopal, A. & Hikosaka, O. Neuronal connections of direct and indirect pathways for stable value memory in caudal basal ganglia. *Eur. J. Neurosci.* **49**, 712–725 (2019).

19. Amita, H., Kim, H. F., Inoue, K.-I., Takada, M. & Hikosaka, O. Optogenetic manipulation of a value-coding pathway from the primate caudate tail facilitates saccadic gaze shift. *Nat. Commun.* **11**, 1876 (2020).
20. Guo, L., Walker, W. I., Ponvert, N. D., Penix, P. L. & Jaramillo, S. Stable representation of sounds in the posterior striatum during flexible auditory decisions. *Nat. Commun.* **9**, 1534 (2018).
21. Chen, A. P. F. *et al.* Nigrostriatal dopamine pathway regulates auditory discrimination behavior. *Nat. Commun.* **13**, 5942 (2022).
22. Menegas, W., Akiti, K., Amo, R., Uchida, N. & Watabe-Uchida, M. Dopamine neurons projecting to the posterior striatum reinforce avoidance of threatening stimuli. *Nat. Neurosci.* **21**, 1421–1430 (2018).
23. Jiang, H. & Kim, H. F. Anatomical Inputs From the Sensory and Value Structures to the Tail of the Rat Striatum. *Front. Neuroanat.* **12**, 30 (2018).
24. Wang, L. & Krauzlis, R. J. Visual Selective Attention in Mice. *Curr. Biol.* **28**, 676-685.e4 (2018).
25. Wang, L., McAlonan, K., Goldstein, S., Gerfen, C. R. & Krauzlis, R. J. A Causal Role for Mouse Superior Colliculus in Visual Perceptual Decision-Making. *J. Neurosci.* **40**, 3768–3782 (2020).
26. Cang, J., Savier, E., Barchini, J. & Liu, X. Visual Function, Organization, and Development of the Mouse Superior Colliculus. *Annu. Rev. Vis. Sci.* **4**, 239–262 (2018).

27. Hikosaka, O. & Wurtz, R. H. Visual and oculomotor functions of monkey substantia nigra pars reticulata. IV. Relation of substantia nigra to superior colliculus. *J. Neurophysiol.* **49**, 1285–1301 (1983).
28. Hikosaka, O., Takikawa, Y. & Kawagoe, R. Role of the basal ganglia in the control of purposive saccadic eye movements. *Physiol. Rev.* **80**, 953–978 (2000).
29. Kaneda, K., Isa, K., Yanagawa, Y. & Isa, T. Nigral inhibition of GABAergic neurons in mouse superior colliculus. *J. Neurosci. Off. J. Soc. Neurosci.* **28**, 11071–11078 (2008).
30. Arcizet, F. & Krauzlis, R. J. Covert spatial selection in primate basal ganglia. *PLoS Biol.* **16**, e2005930 (2018).
31. Ding, L. & Gold, J. I. Caudate encodes multiple computations for perceptual decisions. *J. Neurosci. Off. J. Soc. Neurosci.* **30**, 15747–15759 (2010).
32. Yartsev, M. M., Hanks, T. D., Yoon, A. M. & Brody, C. D. Causal contribution and dynamical encoding in the striatum during evidence accumulation. *eLife* **7**, e34929 (2018).
33. Hormigo, S., Zhou, J., Chabbert, D., Shanmugasundaram, B. & Castro-Alamancos, M. A. Basal Ganglia Output Has a Permissive Non-Driving Role in a Signaled Locomotor Action Mediated by the Midbrain. *J. Neurosci. Off. J. Soc. Neurosci.* **41**, 1529–1552 (2021).
34. Han, X., Vermaercke, B. & Bonin, V. Diversity of spatiotemporal coding reveals specialized visual processing streams in the mouse cortex. *Nat. Commun.* **13**, 3249 (2022).

35. Deniau, J. M., Mailly, P., Maurice, N. & Charpier, S. The pars reticulata of the substantia nigra: a window to basal ganglia output. *Prog. Brain Res.* **160**, 151–172 (2007).

36. Miyamoto, Y. & Fukuda, T. New Subregions of the Mouse Entopeduncular Nucleus Defined by the Complementary Immunoreactivities for Substance P and Cannabinoid Type-1 Receptor Combined with Distributions of Different Neuronal Types. *eNeuro* **9**, ENEURO.0208-22.2022 (2022).

37. Wallace, M. L. *et al.* Genetically Distinct Parallel Pathways in the Entopeduncular Nucleus for Limbic and Sensorimotor Output of the Basal Ganglia. *Neuron* **94**, 138-152.e5 (2017).

38. Takada, M., Tokuno, H., Ikai, Y. & Mizuno, N. Direct projections from the entopeduncular nucleus to the lower brainstem in the rat. *J. Comp. Neurol.* **342**, 409–429 (1994).

39. Joshua, M., Adler, A., Rosin, B., Vaadia, E. & Bergman, H. Encoding of probabilistic rewarding and aversive events by pallidal and nigral neurons. *J. Neurophysiol.* **101**, 758–772 (2009).

40. Turner, R. S. & Anderson, M. E. Context-dependent modulation of movement-related discharge in the primate globus pallidus. *J. Neurosci. Off. J. Soc. Neurosci.* **25**, 2965–2976 (2005).

41. Li, H., Pullmann, D. & Jhou, T. C. Valence-encoding in the lateral habenula arises from the entopeduncular region. *eLife* **8**, e41223 (2019).

42. Li, H. *et al.* Entopeduncular Nucleus Projections to the Lateral Habenula Contribute to Cocaine Avoidance. *J. Neurosci. Off. J. Soc. Neurosci.* **41**, 298–306 (2021).

43. Moriizumi, T., Leduc-Cross, B., Wu, J. Y. & Hattori, T. Separate neuronal populations of the rat substantia nigra pars lateralis with distinct projection sites and transmitter phenotypes. *Neuroscience* **46**, 711–720 (1992).
44. Takada, M. The lateroposterior thalamic nucleus and substantia nigra pars lateralis: Origin of dual innervation over the visual system and basal ganglia. *Neurosci. Lett.* **139**, 153–156 (1992).
45. Kaelber, W. W. & Afifi, A. K. Efferent connexions of the pars lateralis of the substantia nigra (SNL). *J. Anat.* **129**, 405–412 (1979).
46. Todd, K. L., Lipski, J. & Freestone, P. S. Subthalamic nucleus exclusively evokes dopamine release in the tail of the striatum. *J. Neurochem.* **162**, 417–429 (2022).
47. Arnault, P. & Roger, M. The connections of the peripeduncular area studied by retrograde and anterograde transport in the rat. *J. Comp. Neurol.* **258**, 463–476 (1987).
48. Cai, H.-R. *et al.* Comparison of the connectivity of the posterior intralaminar thalamic nucleus and peripeduncular nucleus in rats and mice. *Front. Neural Circuits* **18**, 1384621 (2024).
49. López, H. S. & Carrer, H. F. Investigation of peripeduncular-hypothalamic pathways involved in the control of lordosis in the rat. *Brain Res.* **253**, 287–302 (1982).
50. Factor, E. M., Mayer, A. D. & Rosenblatt, J. S. Peripeduncular nucleus lesions in the rat: I. Effects on maternal aggression, lactation, and maternal behavior during pre- and postpartum periods. *Behav. Neurosci.* **107**, 166–185 (1993).
51. Redgrave, P., Marrow, L. P. & Dean, P. Anticonvulsant role of nigrotectal projection in the maximal electroshock model of epilepsy--II. Pathways from substantia nigra pars

lateralis and adjacent peripeduncular area to the dorsal midbrain. *Neuroscience* **46**, 391–406 (1992).

52. Stefani, A. *et al.* Bilateral deep brain stimulation of the pedunculopontine and subthalamic nuclei in severe Parkinson's disease. *Brain J. Neurol.* **130**, 1596–1607 (2007).
53. Zrinzo, L., Zrinzo, L. V. & Hariz, M. The pedunculopontine and peripeduncular nuclei: a tale of two structures. *Brain J. Neurol.* **130**, e73; author reply e74 (2007).
54. Wang, L., Herman, J. P. & Krauzlis, R. J. Neuronal modulation in the mouse superior colliculus during covert visual selective attention. *Sci. Rep.* **12**, 2482 (2022).
55. McElvain, L. E. *et al.* Specific populations of basal ganglia output neurons target distinct brain stem areas while collateralizing throughout the diencephalon. *Neuron* **109**, 1721-1738.e4 (2021).
56. van der Kooy, D. & Carter, D. A. The organization of the efferent projections and striatal afferents of the entopeduncular nucleus and adjacent areas in the rat. *Brain Res.* **211**, 15–36 (1981).
57. Hikosaka, O. GABAergic output of the basal ganglia. *Prog. Brain Res.* **160**, 209–226 (2007).
58. Nakajima, M., Schmitt, L. I. & Halassa, M. M. Prefrontal Cortex Regulates Sensory Filtering through a Basal Ganglia-to-Thalamus Pathway. *Neuron* **103**, 445-458.e10 (2019).
59. Krauzlis, R. J. *et al.* Visual Psychophysics in Head-Fixed Mice. *Curr. Protoc. Neurosci.* **92**, e95 (2020).

60. Eastman, K. M. & Huk, A. C. PLDAPS: A Hardware Architecture and Software Toolbox for Neurophysiology Requiring Complex Visual Stimuli and Online Behavioral Control. *Front. Neuroinformatics* **6**, (2012).
61. Brainard, D. H. The Psychophysics Toolbox. *Spat. Vis.* **10**, 433–436 (1997).
62. Pelli, D. G. The VideoToolbox software for visual psychophysics: transforming numbers into movies. *Spat. Vis.* **10**, 437–442 (1997).
63. Pachitariu, M., Steinmetz, N., Kadir, S., Carandini, M. & Harris, K. Fast and accurate spike sorting of high-channel count probes with KiloSort. *Adv. Neural Inf. Process. Syst.* **29**, (2016).
64. Subramanian, D., Pearson, J. M. & Sommer, M. A. Bayesian and Discriminative Models for Active Visual Perception across Saccades. *eNeuro* **10**, ENEURO.0403-22.2023 (2023).
65. Franklin, K. B. J. & Paxinos, G. *The Mouse Brain in Stereotaxic Coordinates*. (Elsevier, AP, Amsterdam, 2008).
66. Allen Institute for Brain Science. Allen Reference Atlas. Mouse Brain [P56 Coronal]. Available from atlas.brain-map.org. (2004).

Acknowledgements

This work is supported by the National Eye Institute Intramural Research Program at the National Institutes of Health.

Author Contributions

K.K.C. and R.J.K. conceived the study, designed the experiments, and wrote the manuscript. K.K.C., K.E., and S.M.P. performed the experiments. K.K.C. analyzed the data.

Competing Interests

The authors declare no competing interests.

Figure legends

Figure 1. PS and DMS direct pathways are anatomically distinct but have shared output targets.

A. Viral strategy to dual-label posterior (PS) and dorsomedial (DMS) D1-MSNs using cre-dependent anterograde viruses in D1-cre transgenic mice. B. Injection site of eYFP-expressing virus in DMS (blue). C. Injection site of dsRed-expressing virus in PS (yellow); axonal labeling of DMS-originating D1-MSNs in the entopeduncular nucleus (EP; blue). D. Axonal labeling of PS and DMS -originating D1-MSNs in the substantia nigra (SN). E. Viral strategy to dual label PS and DMS -originating SN disynaptic pathways. F-G. Expression of PS-innervated tdTom-labeled cells in the SN pars lateralis (SNl) and peripeduncular nucleus (PP). Expression of DMS-innervated eYFP-labeled cells in the substantia nigra pars compacta (SNc) and reticulata (SNr). Anatomical boundaries approximated from Franklin & Paxinos Atlas[65]. H-K. Terminal expression of PS→SN (tdTom) and DMS→SN (eYFP) cells in thalamus (H-I) and midbrain (J-K). L. Viral strategy to label the DMS -originating EP disynaptic pathway. M-N. Terminal expression of DMS→EP cells in the midbrain. Scale bars: 500 µm. Abbreviations: AP (anterior-posterior), FG (Fluorogold).

Figure 2. Visual cortex innervates PS more broadly and inclusively than DMS.

A. Injection site of Fluorogold (FG) retrograde tracer in the PS. B-D. PS projecting FG-labeled neurons in visual cortex. E. Injection site of FG in the DMS. F-H. DMS projecting FG-labeled neurons in visual cortex. Cortical divisions approximated from Franklin & Paxinos and Allen Brain Atlases[65,66]. Scale bars: 500 µm. Abbreviations: Au1 (primary

auditory cortex), AuD (dorsal secondary auditory cortex), AuV (ventral secondary auditory cortex), CTX (cortex), Ect (ectorhinal cortex), PrS (presubiculum), RSD (retrosplenial dysgranular cortex), RSG (retrosplenial granular cortex), TeA (temporal association cortex), V1 (primary visual cortex), V2al (anterolateral secondary visual cortex), V2am (anteromedial secondary visual cortex), V2l (lateral secondary visual cortex), V2pm (posteromedial secondary visual cortex).

Figure 3. PS direct pathway activation biases visual decisions.

A. Schematic of spatially cued orientation change-detection task trial structure and left and right visual displays. B. Representative expression of cre-dependent Channelrhodopsin (ChR2-mCherry) and optic fiber placement in the DMS (left) and PS (right) of a Drd1a-cre mouse. C. Schematic of light delivery to DMS or PS during the early delay (left) and late delay or change epochs (right). D. Cumulative lick probabilities from a representative ChR2-expressing Drd1a-cre mouse. The first lick following PS light delivery onset (blue) or at a matched time on non-stimulation trials (gray) was quantified for the early delay epoch (left column) and late delay epoch (right column), separately for contralaterally cued trials (top row) and ipsilaterally cued trials (bottom row). E. Light delivery to the PS during the early delay epoch produced a small but significant increase in lick probability for ChR2-mCherry (purple and gold; N = 6) but not mCherry control (black and gray; N = 4) mice. F. PS Light delivery during the late delay epoch significantly increased lick probability for ChR2-mCherry but not mCherry control mice. G. Light delivery during the change event reduced the median response latency for ChR2-mCherry but not mCherry control mice. Scale bars: 500 µm. Four-way

repeated measures ANOVA (E, F); three-way repeated measures ANOVA (G). Error bars represent standard error of the mean (s.e.m.).

Figure 4. PS direct pathway bias of visual decisions depends on visual context and reward reinforcement.

A. Left: Schematic of visual displays and timing of light delivery for two-patch (late delay) and sequence-arrested one-patch and pink noise control trials. Right: Lick probability observed following PS D1-MSN stimulation paired with the different visual conditions on contralaterally cued trials (N = 6 mice). B. Left: Schematic of operant extinction session structure, with change event paired or unpaired with PS D1-MSN stimulation Right: Omitting rewards for correct detection responses resulted in similar extinction rates for PS D1-MSN stimulation (blue) and non-stimulation (gray) trials. Extinction rates derived from trial hits and misses (open circles; combined sessions of 4 mice). One-way repeated measures ANOVA (A). Error bars represent s.e.m. (A); dashed lines represent 95% confidence intervals (CIs) (B).

Figure 5. PS and DMS direct pathways preferentially modulate SC neurons responsive to visual task properties.

A. Distribution of recorded single units across the superior colliculus (SC) relative to the estimated division of superficial (sSC) and deeper (dSC) layers (n = 530 units; N = 6 mice). B. Left: Peri-stimulus event histograms (PSTHs) of sSC single unit responses to the spatially cued orientation change task stimuli (n = 88). Right: PSTHs of dSC single unit responses with time windows for quantifying task-related activity (n = 442). C.

Percentages of sSC (light gray) and dSC (dark gray) units that exhibited task-related activity. D. Percentages of dSC units exhibiting task properties (colored bars) or not (white bars) that were modulated by optogenetic activation of PS (left) or DMS (right) D1-MSNs. Chi-square tests (C,D). Error bars represent s.e.m. (B) or 95% CI (C,D).

Figure 6. Superior colliculus neuronal responses to PS and DMS direct pathway activation.

A. Spike rasters (top) and mean firing rates (bottom) for example dSC units that were excited (left), inhibited (center), or both excited and inhibited (right) by PS D1-MSN optogenetic stimulation (blue) compared to activity on non-stimulation trials (gray). Optogenetic light delivery indicated by light blue shading. B. Same as A but for dSC units modulated by DMS D1-MSN stimulation. C. Proportions of PS (top) and DMS (bottom) D1-MSN modulated dSC units that were modulated during early delay (white), late delay (dark gray), or both epochs (light gray). D. Left: from recording sessions with both DMS and PS D1-MSN stimulation, proportions of dSC single units that were modulated by PS, DMS or both D1-MSN pathways. Center and right: the type of modulatory effect on dSC firing by PS and DMS D1-MSN stimulation.

Tables

Table 1. Effects of D1-MSN activation on lick probability (related to Figure 3E-F).

	Contra-cued trials		**Ipsi-cued trials**	
	No light	**Light**	**No Light**	**Light**
Mean (s.e.m.)	PS ChR2-mCherry (N = 6)			
Early delay	0.026 (0.004)	0.129 (0.029)	0.043 (0.014)	0.105 (0.031)
Late delay	0.086 (0.026)	0.533 (0.056)	0.083 (0.022)	0.352 (0.053)
	PS mCherry (N = 4)			
Early delay	0.037 (0.032)	0.019 (0.018)	0.061 (0.017)	0.044 (0.032)
Late delay	0.064 (0.047)	0.052 (0.033)	0.031 (0.017)	0.084 (0.081)
	DMS ChR2-mCherry (N = 5)			
Early delay	0.030 (0.011)	0.041 (0.007)	0.064 (0.013)	0.079 (0.021)
Late delay	0.089 (0.018)	0.603 (0.080)	0.100 (0.032)	0.513 (0.103)
	DMS mCherry (N = 4)			
Early delay	0.083 (0.033)	0.058 (0.013)	0.044 (0.005)	0.043 (0.008)
Late delay	0.038 (0.014)	0.075 (0.026)	0.066 (0.017)	0.084 (0.029

	df	**F**	**p**
PS 4-way ANOVA			
Epoch	1,7	48.32	0.0001
Light delivery	1,7	59.93	0.0001
Group	1,7	24.59	0.0011
Cued side	1,7	0.72	0.42
Group x Light	1,7	58.19	0.0001
Group x Epoch	1,7	33.45	0.0004
Epoch x Light	1,7	45.13	0.0001
Group x Light x Cued side	1,7	6.04	0.0394
Group x Light x Epoch	1,7	26.10	0.0009
Group x Light x Cued side x Epoch	1,7	6.67	0.0325
DMS 4-way ANOVA			
Epoch	1,6	20.57	0.0027
Light delivery	1,6	33.23	0.0007
Group	1,6	18.32	0.0037
Cued side	1,6	0.03	0.87
Group x Light	1,6	29.48	0.001
Group x Epoch	1,6	18.15	0.0037
Epoch x Light	1,6	37.53	0.0005
Group x Light x Cued side	1,6	1.30	0.29
Group x Light x Epoch	1,6	26.38	0.0013
Group x Light x Cued side x Epoch	1,6	0.66	0.44

Table 2. Effects of D1-MSN activation on change event reaction time (ms) (related to Figure 3G)

	Contra-cued trials		**Ipsi-cued trials**	
	No light	**Light**	**No Light**	**Light**
Mean (s.e.m.)				
PS ChR2-mCherry (N = 6)	333 (19)	311 (16)	342 (18)	323 (20)
PS mCherry (N = 4)	348 (14)	341 (13)	361 (8)	343 (12)
DMS ChR2-mCherry (N = 5)	334 (21)	320 (18)	352 (18)	328 (15)
DMS mCherry (N = 4)	358 (29)	358 (31)	337 (24)	333 (21)

	df	**F**	**p**
PS 3-way ANOVA			
Light delivery	1,8	50.27	0.0001
Group	1,8	0.78	0.40
Cued side	1,8	2.98	0.12
DMS 3-way ANOVA			
Light delivery	1,7	4.90	0.06
Group	1,7	0.21	0.66
Cued side	1,7	0.27	0.62

Table 3. Percentages (95% CIs) of SC units modulated by task properties and D1-MSN activation (related to Figure 5C-D).

	Cue Event	Delay Activity	Spatial Cue Mod.	Change Event	Lick Activity
All sSC units	78.4 (68.4, 86.5)	46.6 (35.9, 57.5)	18.2 (10.8, 27.8)	18.2 (10.8, 27.8)	1.1 (0.03, 6.2)
All dSC units	55.7 (50.9, 60.4)	37.3 (32.8, 42.0)	20.6 (16.9, 24.7)	22.4 (18.6, 26.6)	6.6 (4.4, 9.3)
PS mod. & Task non-mod. dSC units	21.3 (12.7, 32.3)	21.9 (14.7, 30.7)	22.9 (16.2, 30.7)	19.9 (13.6, 27.4)	27.6 (21.2, 34.6)
PS mod. & Task mod. dSC units	31.5 (23.0, 41.0)	36.1 (25.1, 48.3)	41.3 (27.0, 56.8)	51.1 (35.8, 66.3)	0 (0, 97.5)
DMS mod. & Task non-mod. dSC units	36.1 (26.6, 46.5)	29.0 (21.7, 37.1)	31.4 (24.9, 38.5)	29.4 (22.9, 36.7)	38.9 (32.3, 45.9)
DMS mod. & Task mod. dSC units	36.6 (28.4, 45.5)	49.4 (38.2, 60.6)	62.2 (47.4, 76.1)	62.5 (47.4, 76.1)	10.0 (1.2, 31.7)

Figure 1

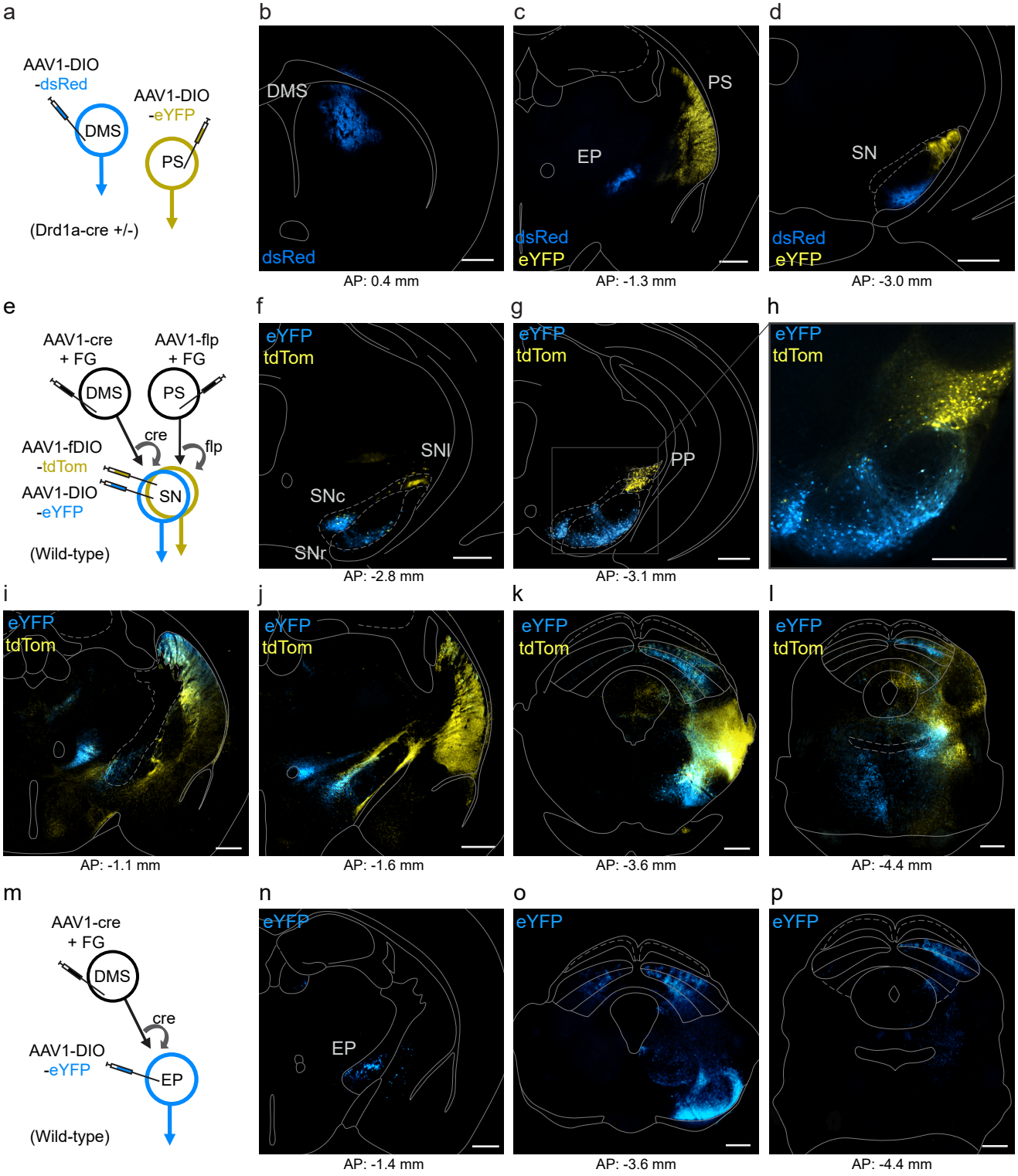
a
AAV1-DIO
-dsRed
AAV1-DIO
-eYFP
DMS
PS
(Drd1a-cre +/-)
b
DMS
dsRed
AP: 0.4 mm
c
PS
EP
dsRed
eYFP
AP: -1.3 mm
d
SN
dsRed
eYFP
AP: -3.0 mm
e
AAV1-cre
+ FG
AAV1-flp
+ FG
DMS
PS
cre
flp
AAV1-fDIO
-tdTom
AAV1-DIO
-eYFP
SN
(Wild-type)
f
eYFP
tdTom
SNl
SNc
SNr
AP: -2.8 mm
g
eYFP
tdTom
PP
AP: -3.1 mm
h
eYFP
tdTom
i
eYFP
tdTom
AP: -1.1 mm
j
eYFP
tdTom
AP: -1.6 mm
k
eYFP
tdTom
AP: -3.6 mm
l
eYFP
tdTom
AP: -4.4 mm
m
AAV1-cre
+ FG
DMS
cre
AAV1-DIO
-eYFP
EP
(Wild-type)
n
eYFP
EP
AP: -1.4 mm
o
eYFP
AP: -3.6 mm
p
eYFP
AP: -4.4 mm

Figure 2

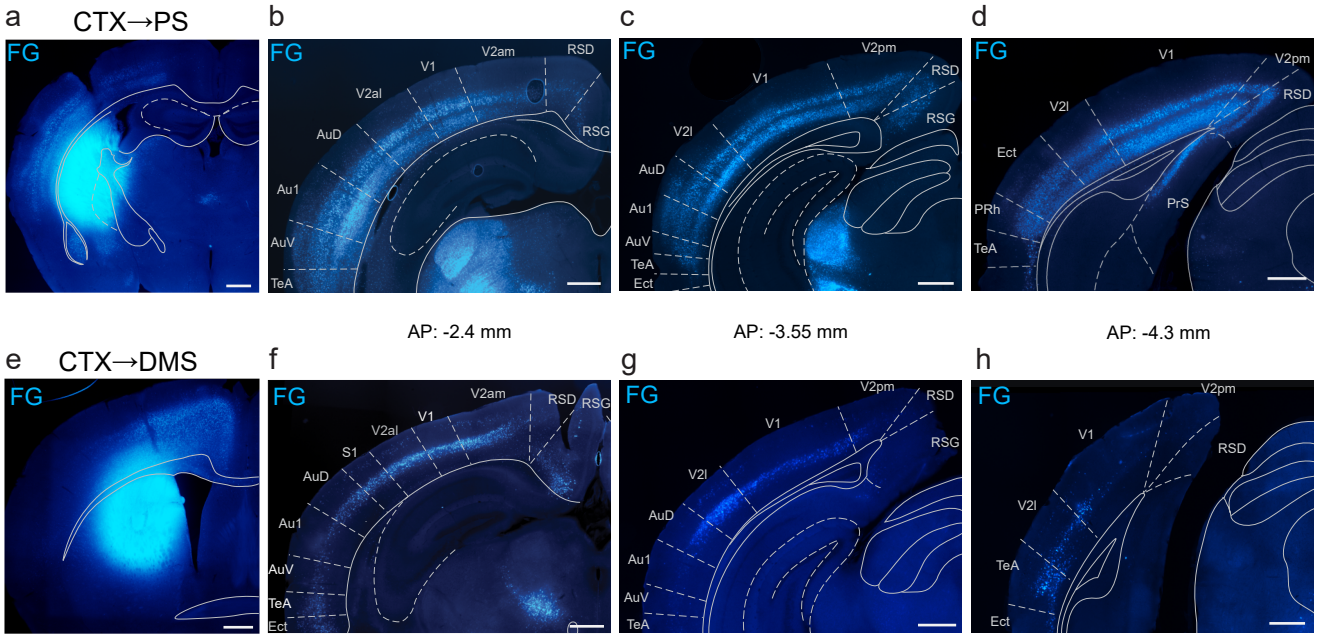
a
CTX→PS
FG
b
FG
V2am
RSD
V1
V2al
AuD
RSG
Au1
AuV
TeA
c
FG
V2pm
V1
RSD
RSG
V2l
AuD
Au1
AuV
TeA
Ect
d
FG
V1
V2pm
V2l
RSD
Ect
PRh
PrS
TeA
AP: -2.4 mm
AP: -3.55 mm
AP: -4.3 mm
e
CTX→DMS
FG
f
FG
V2am
RSD
RSG
V1
V2al
S1
AuD
Au1
AuV
TeA
Ect
g
FG
V2pm
RSD
V1
RSG
V2l
AuD
Au1
AuV
TeA
h
FG
V2pm
V1
RSD
V2l
TeA
Ect

Figure 3

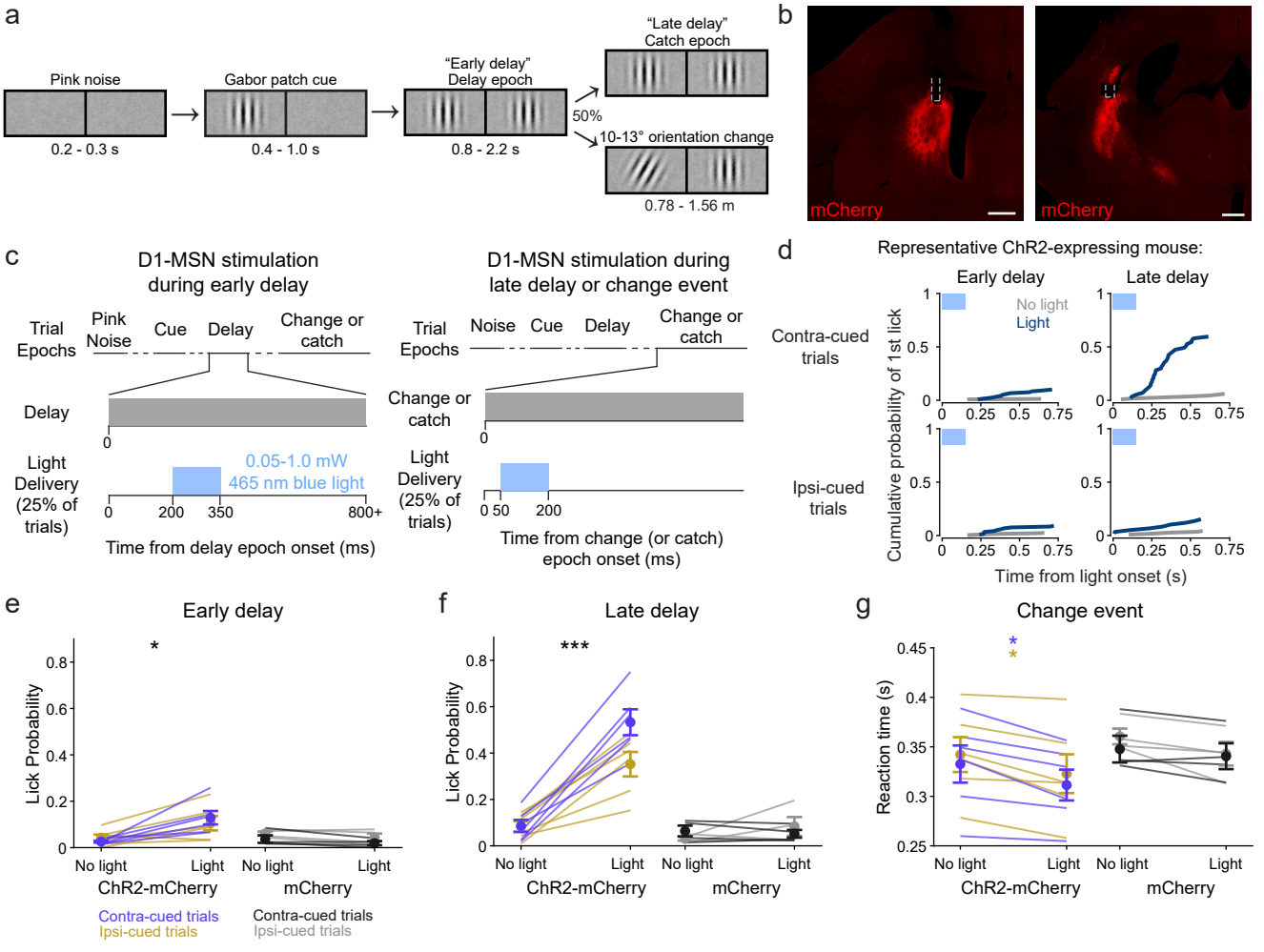
a
Pink noise
0.2 - 0.3 s
Gabor patch cue
0.4 - 1.0 s
"Early delay"
Delay epoch
0.8 - 2.2 s
50%
"Late delay"
Catch epoch
10-13° orientation change
0.78 - 1.56 m
b
mCherry
mCherry
c
D1-MSN stimulation during early delay
Trial Epochs
Pink Noise
Cue
Delay
Change or catch
Delay
Light Delivery (25% of trials)
0.05-1.0 mW
465 nm blue light
0
200
350
800+
Time from delay epoch onset (ms)
D1-MSN stimulation during late delay or change event
Trial Epochs
Noise
Cue
Delay
Change or catch
Change or catch
Light Delivery (25% of trials)
0 50
200
Time from change (or catch) epoch onset (ms)
d
Representative ChR2-expressing mouse:
Early delay
Late delay
No light
Light
Contra-cued trials
Ipsi-cued trials
Cumulative probability of 1st lick
Time from light onset (s)
e
Early delay
Lick Probability
No light
Light
ChR2-mCherry
mCherry
Contra-cued trials
Ipsi-cued trials
f
Late delay
Lick Probability
g
Change event
Reaction time (s)

Figure 4

a

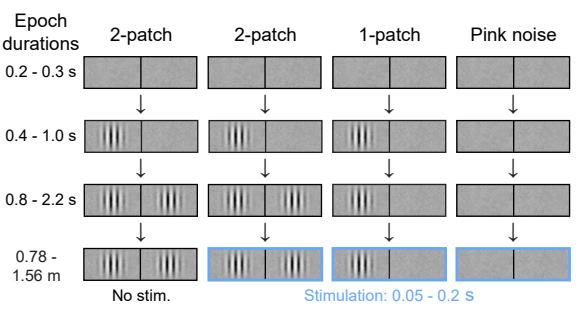
Epoch durations
2-patch
2-patch
1-patch
Pink noise
0.2 - 0.3 s
0.4 - 1.0 s
0.8 - 2.2 s
0.78 - 1.56 m
No stim.
Stimulation: 0.05 - 0.2 s

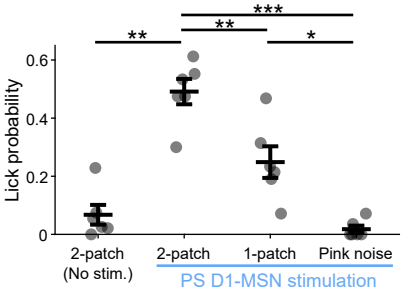
***
**
**
*
Lick probability
0.6
0.4
0.2
0
2-patch (No stim.)
2-patch
1-patch
Pink noise
PS D1-MSN stimulation

b

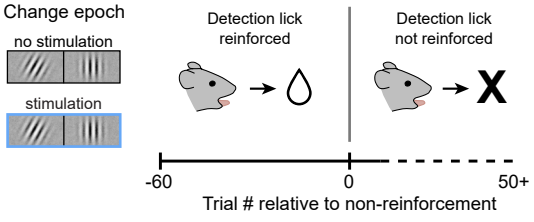
Change epoch
no stimulation
stimulation
Detection lick reinforced
Detection lick not reinforced
X
-60
0
50+
Trial # relative to non-reinforcement

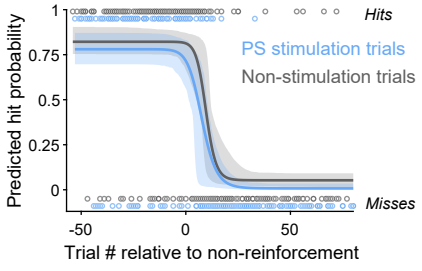
Predicted hit probability
1
0.75
0.5
0.25
0
Hits
Misses
PS stimulation trials
Non-stimulation trials
-50
0
50
Trial # relative to non-reinforcement

Figure 5

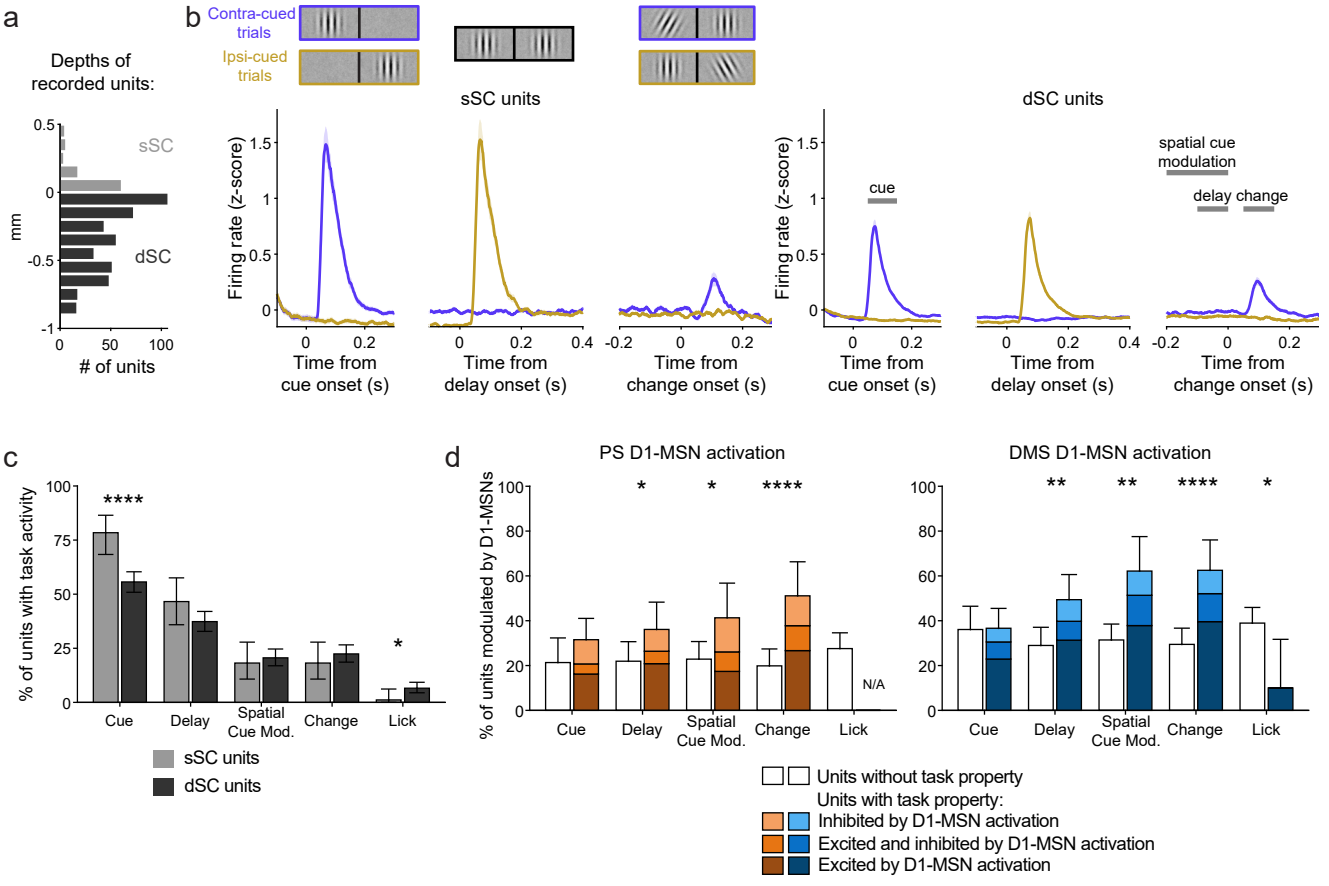
a
Depths of recorded units:
sSC
dSC
mm
# of units
b
Contra-cued trials
Ipsi-cued trials
sSC units
dSC units
Firing rate (z-score)
cue
spatial cue modulation
delay change
Time from cue onset (s)
Time from delay onset (s)
Time from change onset (s)
c
% of units with task activity
Cue
Delay
Spatial Cue Mod.
Change
Lick
sSC units
dSC units
d
PS D1-MSN activation
DMS D1-MSN activation
% of units modulated by D1-MSNs
N/A
Units without task property
Units with task property:
Inhibited by D1-MSN activation
Excited and inhibited by D1-MSN activation
Excited by D1-MSN activation

Figure 6

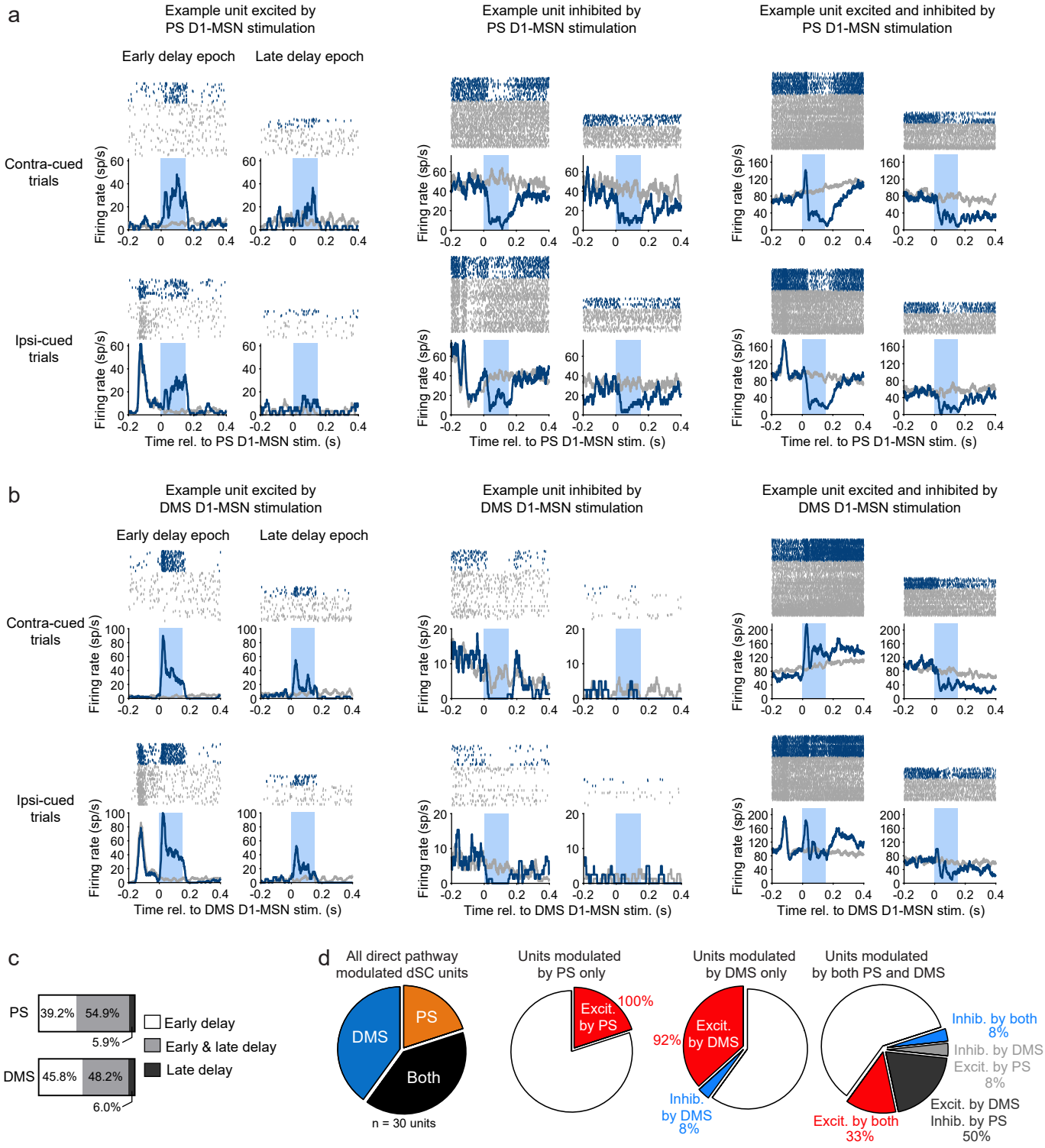
a
Example unit excited by PS D1-MSN stimulation
Example unit inhibited by PS D1-MSN stimulation
Example unit excited and inhibited by PS D1-MSN stimulation
Early delay epoch
Late delay epoch
Contra-cued trials
Ipsi-cued trials
Firing rate (sp/s)
Time rel. to PS D1-MSN stim. (s)
b
Example unit excited by DMS D1-MSN stimulation
Example unit inhibited by DMS D1-MSN stimulation
Example unit excited and inhibited by DMS D1-MSN stimulation
Early delay epoch
Late delay epoch
Contra-cued trials
Ipsi-cued trials
Firing rate (sp/s)
Time rel. to DMS D1-MSN stim. (s)
c
PS
39.2%
54.9%
5.9%
DMS
45.8%
48.2%
6.0%
Early delay
Early & late delay
Late delay
d
All direct pathway modulated dSC units
DMS
PS
Both
n = 30 units
Units modulated by PS only
Excit. by PS
100%
Units modulated by DMS only
Excit. by DMS
92%
Inhib. by DMS 8%
Units modulated by both PS and DMS
Inhib. by both 8%
Inhib. by DMS
Excit. by PS 8%
Excit. by DMS
Inhib. by PS 50%
Excit. by both 33%